# Coherent transfer of quantum information in a silicon double quantum dot using resonant SWAP gates: Supplementary Information

A. J. Sigillito,[1] M. J. Gullans,[1] L. F. Edge,[2] M. Borselli,[2] and J. R. Petta[1]

[1] *Department of Physics, Princeton University, Princeton, New Jersey 08544, USA*

[2] *HRL Laboratories LLC, 3011 Malibu Canyon Road, Malibu, California 90265, USA*

(Dated: October 23, 2019)

## I. THEORETICAL MODEL

The low-energy Hamiltonian for a linear Si/SiGe quantum dot (DQD) array in the presence of a magnetic field gradient and oscillating exchange takes the form [1, 2]

$$H = \sum_i B_i^{\mathrm{tot}} s_i^z + \sum_i J_{i,i+1}[V_{B_{i+1}}(t)]\boldsymbol{s}_i \cdot \boldsymbol{s}_{i+1} \tag{1}$$

where $B_i^{\mathrm{tot}} = B_{\mathrm{ext}} + B_i^M$ is the local magnetic field of spin $i$, $s_i^\mu$ are spin-1/2 operators on site $i$, $J_{i,i+1}$ is the exchange interaction that depends on the AC modulated barrier gate voltage $V_{Bi+1}(t)$. The exchange term will generically have both an ac and dc component due to the positivity of the exchange interaction.

Restricting to a double dot configuration on sites 3 and 4, the states $|\uparrow\uparrow\rangle$ and $|\downarrow\downarrow\rangle$ are exact eigenstates of this Hamiltonian; therefore, it is convenient to isolate an effective two-level system in the $m_z = 0$ subspace $\{|\uparrow\downarrow\rangle, |\downarrow\uparrow\rangle\}$. Denoting the Pauli operators for this two-level system as $\tau_\mu$, the projected Hamiltonian in a local reference frame for qubits 3/4 rotating at frequencies $f_{3/4}$ (note, these are the reference frames for single-qubit EDSR operations on each dot)

$$H_0/h = -\frac{J_{34}}{2}\mathbb{I} + \frac{\Delta_{34}}{2}\tau_z + \frac{1}{2}(j_{34}e^{i\phi - i\delta t}\tau_- + h.c.) \tag{2}$$

where $\Delta_i = B_i - 2\pi f_i$ is the detuning of the magnetic fields, $j_{ii+1}$ is the amplitude of the Fourier component of $J_{ii+1}(t)$ at frequency $f_{\mathrm{SWAP}}$, and $\phi$ is the phase of this ac exchange term relative to the doubly-rotating reference frame of the two spin qubits, $\Delta_{34} = \Delta_3 - \Delta_4$ is the shifted magnetic field gradient, and $\delta/2\pi = f_{\mathrm{SWAP}} - (f_3 - f_4)$ is the detuning of the exchange drive frequency. We assume $f_3 \approx B_3/2\pi > f_4 \approx B_4/2\pi$. In the ideal case, $f_{3,4} = B_{3,4}/2\pi$; however, because of the motion of the electron wavefunction in the magnetic field gradient, we have to take into account possible deviations from this condition. We further assume $f_{\mathrm{SWAP}} \gg j_{34}/2\pi$, so that we are justified in making the rotating wave approximation. This condition is well satisfied in the experiment where the magnetic field gradient is 140 MHz, while the exchange interaction is kept below a few tens of MHz [2].

## II. SWAP TUNEUP AND CALIBRATION

To tune up a linear array of quantum dot spin qubits using the SWAP gate, we use the following approach:

(a) Tune the readout dot (frequency, amplitude, and duration of a $\pi$-pulse)

(b) Perform two-qubit SWAP spectroscopy

(c) Do time-domain SWAP spectroscopy

(d) Repeat items (b) and (c) for each dot in the array

### A. Tune the readout dot

To tune the readout dot, we follow an approach demonstrated many times in the literature and described in the main text. Here we measure the frequency dependence of time-domain Rabi oscillations on the readout dot (colloquially referred to as Rabi chevrons) and shown in Fig. 2(c) in the Main text. From this experiment we extract the readout dot's Rabi frequency and EDSR frequency. These parameters can then be used to apply a $\pi$-pulse on the readout dot.

### B. Two-qubit SWAP spectroscopy

#### *1. One-dimensional frequency domain*

To prepare the array for two-qubit SWAP spectroscopy between dots 3 and 4, we apply a $\pi$-pulse to dot 4 (dot 4 is the readout dot). The $\pi-$pulse on dot 4 leaves the system in the $|\downarrow\uparrow\rangle$ state. We then apply an RF burst on the barrier gate between the two dots ($B_4$) which modulates the exchange coupling between the spins at the frequency $f_{\mathrm{SWAP}}$. $f_{\mathrm{SWAP}}$ is varied and when on resonance, Rabi oscillations are driven between the $|\downarrow\uparrow\rangle$ and $|\uparrow\downarrow\rangle$ states. This leads to some transfer of the spin polarization between dots 3 and 4 which is observed as a dip in the dot 4 spin polarization. An example spectra is shown in Fig. 1. This allows us to directly measure the difference in EDSR frequency between the two dots. The sign of the frequency shift is determined later after the SWAP gate is calibrated, such that Rabi oscillations on dot 3 can be read out.

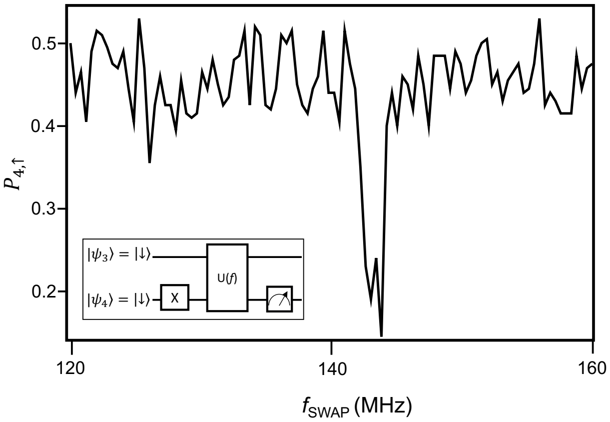


Supplementary Figure 1. SWAP spectroscopy performed on dots 3 and 4. Here $Q_4$ is prepared in the $|\uparrow\rangle$ state and then exchange is modulated at a frequency $f_{\mathrm{SWAP}}$ for 100 $\mu$s by applying a sinusoidal drive to $B_4$. On resonance we observe a dip in $P_{4,\uparrow}$ due to the spin polarization being partially transferred to $Q_3$.

Finding the dip in the SWAP spectra can be challenging for two reasons. First, in isotopically enriched silicon, linewidths can be narrow so a very fine frequency step must be used to ensure that the resonance is not skipped. Secondly, because the RF burst is coherent, it is possible to choose some burst length and power that leads to approximately an even integer number of SWAP oscillations (equivalent to identity). In this case the constrast in the spectra will be low. For these reasons one can use chirped RF bursts which when applied for short durations can lead to broadening of the resonance, thus reducing the number of points one must take. By applying the RF burst for long periods of time, the pulses can be made adiabatic, which offers high measurement contrast.

### 2. *Two-dimensional amplitude and frequency domain*

With the SWAP frequency determined (∼140 MHz in the main text), we prepare the $|\downarrow\uparrow\rangle$ state and apply an RF burst to $B_4$, varying both the amplitude and frequency of the RF drive. The RF burst length is fixed at 600 ns. An example spectra is shown in Fig. 2(b) of the main text. By choosing the appropriate frequency and burst amplitude (dip in $P_{4,\uparrow}$), we can apply a two-qubit SWAP gate to within two-qubit Ising phases (described below) and single-qubit $z$ rotations. This initial calibration is sufficient for high fidelity readout and transfer of spin polarization in an array following the procedure oulined in Fig. 2 and discussed in the main text.

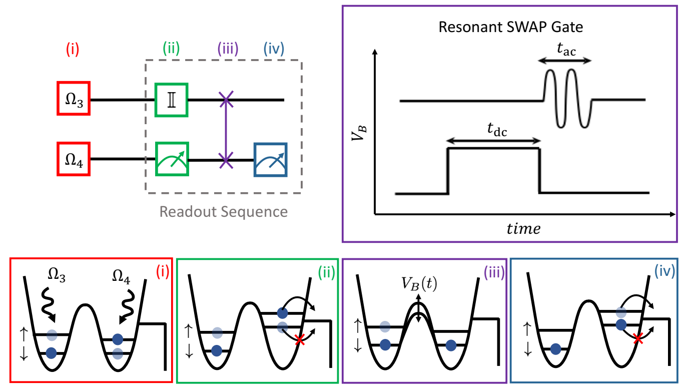


Supplementary Figure 2. Typical pulse sequence for reading out two qubits. We first prepare the system in some state by applying a rotation $\Omega_i$ on qubit $i$ during phase (i). The readout dot (dot 4) is then brought into resonance with the lead and measured through spin dependent tunneling (ii). A resonant SWAP is applied at time (iii) after which the second dot (dot 3) is read out (iv). The time dependent voltage on the barrier for a resonant SWAP gate is shown to the upper right. Here $t_{\mathrm{DC}} = 0$ for readout, but $t_{\mathrm{DC}}$ can be non-zero when applying a pure SWAP gate while running a quantum algorithm.

## III. SWAP CALIBRATION

The resonant SWAP gate is realized by simply driving the exchange field at the resonance condition $f_{\mathrm{SWAP}} = |B_3 - B_4|$ for a time $t_{\mathrm{AC}} = \pi/j_{34}$. A straightforward calculation shows that the total unitary for the pulse in the $\{|\uparrow\downarrow\rangle, |\downarrow\uparrow\rangle\}$ subspace is

$$\begin{aligned} U_0 = \Bigg[ &\cos\left(\frac{\Omega_{\mathrm{ex}} t_{\mathrm{ac}}}{2}\right)\mathbb{I} - i\Bigg(\frac{\Delta_{34}^{\mathrm{ac}} - \delta}{\Omega_{\mathrm{ex}}}\tau_z \\ &+ \frac{j_{34}}{\Omega_{\mathrm{ex}}}(\cos\phi\,\tau_x + i\sin\phi\,\tau_y)\Bigg)\sin\left(\frac{\Omega_{\mathrm{ex}} t_{\mathrm{ac}}}{2}\right)\Bigg] \\ &\times e^{i(J_{34}^{\mathrm{dc}} t_{\mathrm{dc}} + J_{34}^{\mathrm{ac}} t_{\mathrm{ac}})/2} e^{-i\Delta_{34}^{\mathrm{dc}} t_{\mathrm{dc}} \tau_z/2}, \end{aligned} \tag{3}$$

$$\Omega_{\mathrm{ex}} = \sqrt{(\Delta_{34}^{\mathrm{ac}} - \delta)^2 + j_{34}^2}, \tag{4}$$

where $\Omega_{\mathrm{ex}}$ is the effective Rabi frequency of the ac exchange term, $J_{34}^{\mathrm{dc/ac}}$ is the static exchange during the dc/ac portion of the gate, and $\Delta_{34}^{\mathrm{dc/ac}}$ is the detuning of the gradient during the dc/ac portion of the gate. These distinctions between the two gate segments are necessary because the local magnetic field on each dot undergo small shifts as the gate voltages are adjusted due to changes in the position of the electron wavefunctions in the magnetic gradient. To cancel out the dc Ising phase, we require $e^{i(J_{34}^{\mathrm{dc}} t_{\mathrm{dc}} + J_{34}^{\mathrm{ac}} t_{\mathrm{ac}})/2} = i$, leading to the timing condition

$$t_{\mathrm{dc}} = \frac{(4n+1)\pi}{J_{34}^{\mathrm{dc}}} - \frac{t_{\mathrm{ac}} J_{34}^{\mathrm{ac}}}{J_{34}^{\mathrm{dc}}}, \tag{5}$$

for some $n = 0, 1, 2, \ldots$. In the ideal case when $\Delta_{34}^{\mathrm{ac}} = \delta$, $t_{\mathrm{ac}} = \pi/j_{34}$, and $t_{\mathrm{dc}}$ satisfies Eq. (5), the total unitary, including the evolution in the spin-polarized states, is given by

$$
\begin{aligned}
U &= Z_3(\theta_3) Z_4(\theta_4)\mathrm{SWAP}, && (6)\\
\theta_3 &= \frac{(\Delta_3^{\mathrm{dc}} + \Delta_4^{\mathrm{dc}})t_{\mathrm{dc}}}{2} - \frac{\Delta_{34}^{\mathrm{dc}}}{2} t_{\mathrm{dc}} \\
&+ \frac{(\Delta_3^{\mathrm{ac}} + \Delta_4^{\mathrm{ac}})t_{\mathrm{ac}}}{2} + \phi, && (7)\\
\theta_4 &= \frac{(\Delta_3^{\mathrm{dc}} + \Delta_4^{\mathrm{dc}})t_{\mathrm{dc}}}{2} + \frac{\Delta_{34}^{\mathrm{dc}}}{2} t_{\mathrm{dc}} \\
&+ \frac{(\Delta_3^{\mathrm{ac}} + \Delta_4^{\mathrm{ac}})t_{\mathrm{ac}}}{2} - \phi. && (8)
\end{aligned}
$$

Calibration of the gate requires a precise measurement of $J_{34}^{\mathrm{dc/ac}}$ and $\theta_{3/4}$. Both classes of errors can be calibrated using the gate sequences shown in Fig. 3(a)-(b). The probability of measuring spin up on the right qubit after the pulse sequence in Fig. 3(a) with an $X/2$ gate on the left qubit before $U$, a $-X/2$ gate on the right qubit after $U$, and an identity or $X$ pulse on the right qubit after $U$ is given by

$$
\begin{aligned}
p_\uparrow &= \frac{1}{2} + \frac{1}{2}\sin\Big[\Big(\Delta_3^{\mathrm{dc}} - \frac{J_{34}^{\mathrm{dc}}}{2}\Big)t_{\mathrm{dc}} \\
&+ \frac{\Delta_3^{\mathrm{ac}} + \Delta_4^{\mathrm{ac}}}{2} t_{\mathrm{ac}} - \frac{J_{34}^{\mathrm{ac}}}{2} t_{\mathrm{ac}} - \phi\Big], && (9)\\
p_\uparrow &= \frac{1}{2} - \frac{1}{2}\sin\Big[\Big(\Delta_3^{\mathrm{dc}} + \frac{J_{34}^{\mathrm{dc}}}{2}\Big)t_{\mathrm{dc}} \\
&+ \frac{\Delta_3^{\mathrm{ac}} + \Delta_4^{\mathrm{ac}}}{2} t_{\mathrm{ac}} + \frac{J_{34}^{\mathrm{ac}}}{2} t_{\mathrm{ac}} - \phi\Big], && (10)
\end{aligned}
$$

respectively. For the pulse sequence in Fig. 3(b), the left qubit spin up probability with an $X/2$ gate on the right qubit before $U$, a $-X/2$ gate on the left qubit after $U$, and an identity or $X$ pulse on the left qubit after $U$ is given by

$$
\begin{aligned}
p_\uparrow &= \frac{1}{2} + \frac{1}{2}\sin\Big[\Big(\Delta_4^{\mathrm{dc}} - \frac{J_{34}^{\mathrm{dc}}}{2}\Big)t_{\mathrm{dc}} \\
&+ \frac{\Delta_3^{\mathrm{ac}} + \Delta_4^{\mathrm{ac}}}{2} t_{\mathrm{ac}} - \frac{J_{34}^{\mathrm{ac}}}{2} t_{\mathrm{ac}} + \phi\Big], && (11)\\
p_\uparrow &= \frac{1}{2} - \frac{1}{2}\sin\Big[\Big(\Delta_4^{\mathrm{dc}} + \frac{J_{34}^{\mathrm{dc}}}{2}\Big)t_{\mathrm{dc}} \\
&+ \frac{\Delta_3^{\mathrm{ac}} + \Delta_4^{\mathrm{ac}}}{2} t_{\mathrm{ac}} + \frac{J_{34}^{\mathrm{ac}}}{2} t_{\mathrm{ac}} + \phi\Big], && (12)
\end{aligned}
$$

respectively. Thus, by varying $t_{\mathrm{dc}}$ in the application of $U$, one can determine $\Delta_{3/4}^{\mathrm{dc}}$, $J_{34}^{\mathrm{dc/ac}}$, $(\Delta_3^{\mathrm{ac}} + \Delta_4^{\mathrm{ac}})/2$, and $\phi$ from these four measurements combined with similar measurements where the gate on the right qubit following $U$ is a $-Y/2$ gate. As a result, these eight measurements are sufficient for calibrating $\theta_i$ and $t_{\mathrm{dc}}$ to realize a pure resonant SWAP gate.

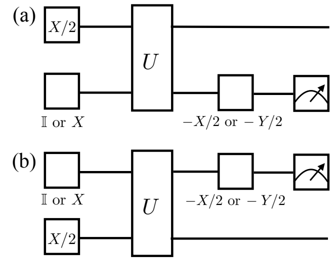


Supplementary Figure 3. Calibration protocol of SWAP gate $U$ to measure the static exchange terms $J_{34}^{\mathrm{dc/ac}}$ and the residual single-qubit phases $\theta_i$. In (a)-(b) we effectively perform a Ramsey experiment except that, in between the two $\pi/2$ pulses, we swap the state of the left and right qubits. These two pulse sequences allows us to measure $J_{34}^{\mathrm{dc/ac}}$ and $\theta_i$ by varying $t_{dc}$ and changing the input state of the other qubit.

## IV. EXTRACTING FIDELITY FOR PROJECTION-SWAP

In Fig. 3 of the main text, the *projection*-SWAP is benchmarked. The experiment begins by initializing $Q_3$ and $Q_4$ in the $|\downarrow\downarrow\rangle$, $|\downarrow\uparrow\rangle$, $|\uparrow\downarrow\rangle$, and $|\uparrow\uparrow\rangle$ states then applying *projection*-SWAP gates $N$ times. Each gate is separated by a 100 ns idle. After applying the SWAP gates, the state of $Q_3$ and $Q_4$ are measured and the probability of measuring spin up $P_{i,\uparrow}$ is plotted as a function of $N$. For a large number of $N$ we expect the integrated error to leave the qubits in a mixed state with $P_{i,\uparrow}$=0.5. For small $N$, $P_{i,\uparrow}$ oscillates with a period of 2 for the antiparallel spin input states. Because $N$ is an integer, the decay appears as two curves in the main text. To clearly demonstrate the oscillations, we plot a small region of the data using a solid line as shown in Fig. 4. In all cases we take the decay to be of the form $f_{i,s_3 s_4}^N$, where $f_{i,s_3 s_4}$ is the fidelity of the SWAP for input state $|s_3 s_4\rangle$. Explicitly, we fit the decays to

$$
\begin{cases}
P_{i,\uparrow} = -A f_{i,\downarrow\downarrow}^N + B & |\psi_3, \psi_4\rangle_{\mathrm{in}} = |\downarrow\downarrow\rangle \\
P_{i,\uparrow} = (-1)^{(N+c)} A f_{i,\downarrow\uparrow}^N + B & |\psi_3, \psi_4\rangle_{\mathrm{in}} = |\downarrow\uparrow\rangle \\
P_{i,\uparrow} = (-1)^{(N+c+1)} A f_{i,\uparrow\downarrow}^N + B & |\psi_3, \psi_4\rangle_{\mathrm{in}} = |\uparrow\downarrow\rangle \\
P_{i,\uparrow} = A f_{i,\uparrow\uparrow}^N + B & |\psi_3, \psi_4\rangle_{\mathrm{in}} = |\uparrow\uparrow\rangle
\end{cases}
\qquad (13)
$$

where $c = 1(2)$ for $Q_{3(4)}$, $A$ is half the measurement visibility, and $B$ is an offset given by the dark count. The prefactor accounts for the phase of the oscillations determined by the input state and the qubit being measured. The fully-spin-polarized states are not expected to oscillate. The extracted fidelities $F_{s_3 s_4}^{(p)} = \frac{1}{2}(f_{3,s_3 s_4} + f_{4,s_3 s_4})$ are summarized in Fig. 3 of the main text.

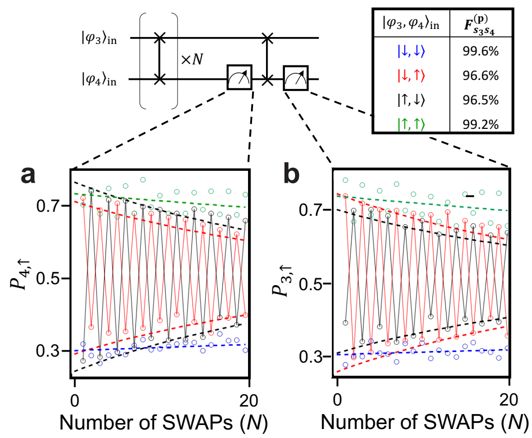


Supplementary Figure 4. A zoomed-in region of Fig. 3 of the main text is plotted using solid lines to highlight the oscillations between the $|\downarrow\uparrow\rangle$ and $|\uparrow\downarrow\rangle$ states. The data in panel (a) corresponds to measurements on $Q_4$ whereas the data in panel (b) are measurements of $Q_3$ using the *projection*-SWAP readout scheme.

## V. STATE TOMOGRAPHY

State tomography was performed on both qubits before and after applying a SWAP gate as shown in Fig. 4(a) of the main text. A $\pi/2$ rotation was applied to $Q_3$ and $Q_4$ was prepared in the $|\downarrow\rangle$ state. For simplicity, the imaginary component of the density matrix is not plotted in the main text, but was extracted and is used in the calculation of state fidelity. We include the imaginary component of the density matrices here in Fig. 5.

In parallel to the state tomography, the measurement visibility for $Q_3$ and $Q_4$ was monitored by preparing $|\downarrow\downarrow\rangle$ and $|\uparrow\uparrow\rangle$ such that state preparation and measurement errors could be subtracted out following the procedures outlined in [2] and [3]. In this approach, we first define a measurement fidelity $F_{(i,j)}$ where the subscript $i$ denotes the qubit and $j$ denotes the spin state. We then correct the single-spin density matrices $\rho_{\text{raw},i}$ by mutiplying them by the correction matrix $\hat{F}_i$. The corrected density matrices are then given by

$$\rho_i = \hat{F}\rho_{\text{raw},i} \tag{14}$$

with

$$\hat{F}_i = \begin{pmatrix} F_{(i,|\downarrow\rangle)} & 1 - F_{(i,|\uparrow\rangle)} \\ 1 - F_{(i,|\downarrow\rangle)} & F_{(i,|\uparrow\rangle)} \end{pmatrix}. \tag{15}$$

Here we measure a visibility ranging from $P_{3,\uparrow} = 0.27$ to $P_{3,\uparrow} = 0.73$ and $P_{4,\uparrow} = 0.22$ to $P_{4,\uparrow} = 0.78$.

## VI. EXPERIMENTAL SETUP

The experiment timing was controlled using a Tektronix AWG5008 arbitrary waveform generator. Channels 1-4 were used for microwave pulse upconversion and shaping and were connected to the $I$ and $Q$ inputs of a home-built microwave vector modulation box. Channel 5 was used to control the exchange pulses.

The local oscillator(LO) which defines the reference frame for each qubit was provided by a Holzworth 4

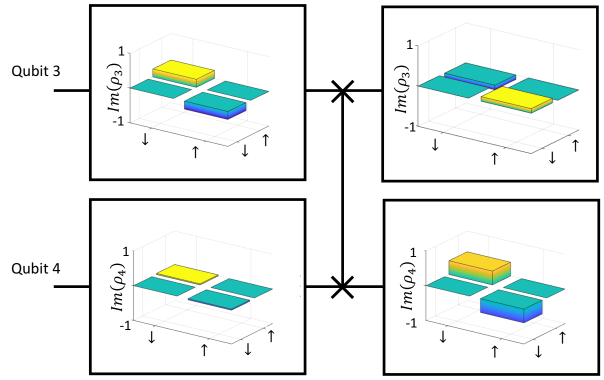


Supplementary Figure 5. Imaginary component of the density matrices presented in Fig. 4(a) of the main text.

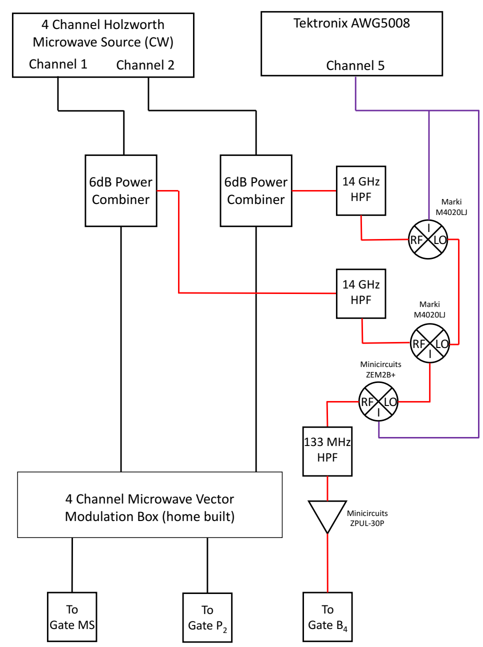


Supplementary Figure 6. Partial schematic of experimental setup highlighting mixing technique used to generate AC fields coherent with doubly-rotating two-qubit reference frame. Exchange pulses are generated in the red arm of the schematic and amplitude modulated using Tektronix AWG5208.

channel microwave source operated as a continuous wave (CW) source. To ensure that the exchange pulses were phase-coherent with the local oscillators of the microwave sources (and thus with the qubits), the local oscillators driving qubits 3 and 4 were fed into a mixer and their beat frequency was used to construct the RF exchange pulse. The signal was chopped using two additional microwave mixers and the resulting signal was amplified and applied to the barrier gate controlling exchange. A partial experiment schematic highlighting the mixing scheme (in red) is shown in Fig. 6. This setup could be improved by replacing two of the mixers with a high-speed microwave switch and by incorporating a programmable attenuator in series with the amplifier to help decouple the tuning of the single- and two-qubit gates. In the current scheme, changing the LO power of one qubit affects both the Rabi frequency of that qubit and the amplitude of the two-qubit exchange pulse.

[1] M. Russ, D. M. Zajac, A. J. Sigillito, F. Borjans, J. M. Taylor, J. R. Petta, and G. Burkard, Phys. Rev. B **97**, 085421 (2018).

[2] D. M. Zajac, A. J. Sigillito, M. Russ, F. Borjans, J. M. Taylor, G. Burkard, and J. R. Petta, Science **359**, 439 (2018).

[3] T. F. Watson, S. G. J. Philips, E. Kawakami, D. R. Ward, P. Scarlino, M. Veldhorst, D. E. Savage, M. G. Lagally, M. Friesen, S. N. Coppersmith, M. A. Eriksson, and L. M. K. Vandersypen, Nature **555**, 633 (2018).